EFFECT OF CRACK-TIP PLASTIC ZONE ON KINKED OR BRANCHED CRACK GROWTH

H. HORII* and S. NEMAT-NASSER**

It has been noted that crack growth phenomena, such as unstable initiation, kinking, and branching, are strongly affected by, or have even resulted from, the presence of a plastic zone and an associated residual strain at the original crack tip. As typical examples of this kind of crack growth, the crack branching of a mode I crack and the unstable crack initiation from the ends of a shear crack under compression are considered. For both cases, an analytical model is developed, and numerical results are obtained in order to show the interplay between plasticity and fracturing.

EFFECT OF CRACK-TIP PLASTICITY ON CRACK BRANCHING

To analyze the branching of a running crack, the stress distribution around the crack tip has been investigated, and the fact that the maximum tangential stress moves out of the plane of crack propagation at high velocities has been reported. However, both the predicted crack branching angle and the estimated crack tip velocity at branching appear to be higher than those observed in experiments. Experimental observations have shown that there is no single instance of crack branch initiation; in fact, there are multiple branching attempts in the crack branching process; see e.g. [1,2]. The possibility that crack branching is the result of the nucleation and coalescence of many interacting microcracks has also been pointed out. It is noted that the model of crack branching must be based on the associated microevents at the crack tip[3]. In the literature, however, there seems to exist no attempt to consider the effect of plastic deformation at the running crack tip on the branching phenomena. In the present work, we consider the effect of a crack-tip plastic zone on crack branching. To simplify the analysis, a static problem is studied.

* Associate Professor, Dept. of Civil Eng., University of Tokyo, Japan
** Professor, Dept. of Applied Mechanics and Engineering Sciences, University of California, San Diego, U. S. A.

Branching Crack with Plastic Zone

There are numbers of reports to show the importance of the microevents at the running crack tip for its bifurcation; see e.g. [3]. In this work, to avoid the difficulties in identification and modeling of the microevents and complication in the dynamic formulation, we treat a static problem and we consider only the plastic zone (caused by a static loading) as crack-tip microevents.

Horii, Hasegawa, and Nishino[4,5] report the significance of the residual strain on the crack initiation with a model shown in Fig. 1. It is shown that the stress intensity factor at the tip of the extended crack is reduced because of the residual strain in the plastic zone. As a consequence, some energy must be supplied to initiate the unstable crack growth. For brittle materials the required energy for the crack initiation is small and the Griffith criterion turns out to be valid even with the plastic zone at the original crack tip. With increasing ductility of the material, the required energy for the crack initiation increases drastically, which may lead to the stable crack growth.

In this paper we consider a model shown in Fig. 2 to investigate the effect of the plastic deformation at the tip of the original crack on the crack branching. Comparing results with those obtained for the model shown in Fig. 1b, we examine the possibility of the change in crack branching features because of the microevents at the crack tip.

Analytic Model

First we consider the distribution of the plastic strain at the tip of the original crack; see Fig. 1a. The length of the plastic zone, which makes an angle θ with the x-axis, is denoted by ℓ_p. The boundary conditions are

$$\sigma_y = \tau_{xy} = 0, \qquad \text{on OQ,} \tag{1}$$

$$u_y^+ = u_y^-, \quad \tau_{r\theta} = \tau_Y, \qquad \text{on OP and OP'} \tag{2}$$

where τ_Y denotes the yield stress in shear. The condition at the end of the plastic zone,

$$\text{stress is bounded at P and P',} \tag{3}$$

must be satisfied. As a loading parameter, we introduce the "applied K-value" K_{IA} which is the stress intensity factor when no plastic zones exist at the crack tip. With the given value of K_{IA}, the length of the plastic zone and the distribution of plastic strain (slip) are obtained as a solution of the problem stated above.

Next, with the obtained distribution of the residual strain, we calculate the stress intensity factor at the tip of the branched crack; see Fig. 2. In this problem the additional boundary conditions

$$\sigma_\theta = \tau_{r\theta} = 0, \qquad \text{on OQ and OQ'} \tag{4}$$

are assumed. Solving the second problem, we obtain the stress intensity factors at the tips of the branched cracks for given values of Φ and ℓ_t/ℓ_p.

Formulation

Muskhelishvili's complex stress functions Φ and Ψ are employed. For a single dislocation at z_0 near a semi-infinite crack, we introduce stress functions $\Phi_D=\Phi_0+\Phi_R$ and $\Psi_D=\Psi_0+\Psi_R$ where Φ_0 and Ψ_0 are stress functions for a single dislocation in an infinite plane and Φ_R and Ψ_R are the complementary potentials to satisfy the stress free condition (1). Φ_R and Ψ_R are obtained by the method of Muskhelishvili[4,5]. They are given by

$$\begin{aligned}
\Phi_0' &= \frac{\alpha}{z - z_0}, \qquad \Psi_0' = \frac{\bar{\alpha}}{z - z_0} + \frac{\alpha \bar{z}_0}{(z - z_0)^2}, \\
\Phi_R' &= -\alpha[F(z, z_0) + F(z, \bar{z}_0)] - \alpha(z_0 - \bar{z}_0)G(z, \bar{z}_0), \\
\Psi_R' &= \bar{\Phi}_R' - \Phi_R' - z\Phi_R'',
\end{aligned} \tag{5}$$

with

$$F(z, z_0) = \frac{1}{2}\left[1 - \sqrt{\frac{z_0}{z}}\right]/(z - z_0), \quad G(z, z_0) = \frac{\partial}{\partial z_0} F(z, z_0), \tag{6}$$

where $\alpha=\mu([u_r]+i[u_\theta])e^{i\theta}/\pi i(\kappa+1)$, $[u]=u^+-u^-$, and $\bar{\Phi}=\overline{\Phi(\bar{z})}$.

Stress functions Φ_D and Ψ_D automatically satisfy the stress free condition (1) on the crack surface. We introduce distributed dislocations along the plastic zones OP and OP'; see Fig. 1a. From (2)-1 (the first equation of (2)) and the symmetry of the problem, the dislocation density is given by

$$\begin{aligned}
\alpha(\xi) &= -i\beta_p(\xi)e^{i\theta}, \qquad \text{at } z_0 = \xi e^{i\theta}, \text{ and} \\
\alpha(\xi) &= i\beta_p(\xi)e^{-i\theta}, \qquad \text{at } z_0 = \xi e^{-i\theta},
\end{aligned} \tag{7}$$

where $\beta_p(\xi)$ is a real function to be determined. The yield condition along the plastic zone, (2)-2, leads to the singular integral equation for the dislocation density $\beta_p(\xi)$,

$$-2\int_0^{\ell_p}\frac{\beta_p(\xi)}{\xi-\eta}d\xi+\int_0^{\ell_p}\beta_p(\xi)K(\xi,\eta;\theta)d\xi+\frac{K_{IA}}{\sqrt{2\pi\eta}}\frac{1}{2}\sin\theta\cos\frac{\theta}{2}=\tau_Y, \quad (8)$$

where

$$K(\xi,\eta;\theta)=\mathrm{Re}\{e^{4i\theta}[\frac{2}{\xi-\eta e^{2i\theta}}+\frac{2i\eta\sin 2\theta}{(\xi-\eta e^{2i\theta})^2}]\}$$
$$+4\eta\sin^2\theta\,\mathrm{Re}\{e^{2i\theta}[F'(z,z_0)+F'(z,\overline{z_0})$$
$$-\xi\{e^{-i\theta}G'(z,\overline{z_0})+e^{i\theta}G'(z,z_0)\}]\}, \quad (9)$$

with Re{ } for the real part of the argument; $F'=\frac{\partial}{\partial z}F$.

Solving (8) for the dislocation density $\beta_p(\xi)$ numerically with the condition (3), we obtain

$$K_{IA}/\tau_Y\sqrt{\pi\ell_p}=2.35 \quad \text{for } \theta=76.1^\circ, \quad (10)$$

which provides the relation between ℓ_p and K_{IA}. The orientation of the plastic zone is set to be 76.1° such that the dissipated plastic work is maximized for a constant K_{IA}.

With the obtained distributed dislocations as the residual strain, the solution to the second problem (Fig. 2) is formulated as follows. Using the solution for a dislocation near a semi-infinite crack, (5) and (6), the branched portion of the crack OR and OR' are replaced with distributed dislocations (density is given by (7) with complex function $\beta_t(\xi)$ and Φ). With the presence of the residual strain (dislocations with the obtained density β_p) along OP and OP' and the external loading K_{IA}, the stress free conditions (4) lead to a singular integral equation for dislocation density β_t,

$$-2\int_0^{\ell_t}\frac{i\overline{\beta}_t}{\xi-\eta}d\xi+\int_0^{\ell_t}\{\beta_t K_1(\xi,\eta,\Phi)+\overline{\beta}_t K_2(\xi,\eta,\Phi)\}d\xi$$
$$+\int_0^{\ell_p}\beta_p K_p(\xi,\eta,\theta,\Phi)d\xi+\frac{K_{IA}}{\sqrt{2\pi\eta}}\cos\frac{\Phi}{2}(\cos^2\frac{\Phi}{2}+\frac{i}{2}\sin\Phi)=0, \quad (11)$$

where K_1, K_2, K_p are obtained similarly to (9) with (5) and (6); lengthy expressions for them are omitted.

Solving (11) numerically, the stress intensity factor at the tip R and R' are obtained, using the relation between β_t and K_I, K_{II}.

Results

The values of the stress intensity factors are plotted in Fig. 3 as functions of the branching angle Φ for indicated values of ℓ_t/ℓ_p. The limiting value of K_I at large ℓ_t/ℓ_p (no plastic zones) agrees with numerical results by Lo[6]. At large values of ℓ_t/ℓ_p, K_I attains the peak value at Φ = 25-30°; the angles for K_{Imax} and K_{II}= 0 are close. With decreasing value of ℓ_t/ℓ_p the peak value of K_I decreases while the critical angle Φ does not show drastic variation. Although the stress distribution at the crack tip is very different due to the residual strain, the critical branching angle is not affected by the crack tip plasticity.

In Fig. 4 the variation of the maximum value of K_I with ℓ_t/ℓ_p is shown with results for the straight crack extension (Fig. 1b). It is seen that K_I value is less than that for the case with no plastic zone ($\ell_t/\ell_p = \infty$) because of the residual strain in the plastic zone. The value of K_I for the branched crack is less than that for the straight extension at all values of ℓ_t/ℓ_p. For the static calculation of the problem shown in Fig. 4, no indication is observed for the possibility of the branching rather than straight crack extension. In addition, note that the required energy for the crack branching can be calculated from this result; see [4,5].

In this work calculations are only for static problems and only the crack tip plasticity is considered as microevents. There seems to exist a possibility that the inclusion of the dynamic effects and other models of microevents may lead to results which provide a crack branching condition.

MICROMECHANISM OF BRITTLE-DUCTILE TRANSITION

Another example of phenomena caused by the interaction between crack growth and plastic deformation appears to be the underlying micromechanism of the transition from the brittle to the ductile mode of failure that is observed under increasing confining pressure in solids containing microdefects. The slip along the initial flaw, caused by the applied farfield compression, results in the formation of plastic zones and tension cracks at the ends of the initial flaw; see Horii and Nemat-Nasser[7].

Fig. 5a shows a single flaw in a Columbia resin CR39 plate compressed with constant stress ratio. Because of

the presence of the lateral confinement the growth of tension cracks is arrested. The residual strain distribution in the unloaded specimen is shown by the photoelastic picture on Fig. 5b. It is seen that extensive plastic flow has occurred. On the basis of this observation we shall present a mathematical model for brittle-ductile transition.

Model of Brittle-Ductile Transition

The mathematical model is shown in Fig. 6. It consists of the frictional and cohesive flaw PP' which has produced, at its tips, tension cracks PQ and P'Q', as well as collinear plastic slips PR and P'R'. The boundary conditions on the initial flaw, the cracks, and the plastic zones are

$$u_y^+ = u_y^-, \quad \tau_{xy} = -\tau_c + \mu\sigma_y, \quad \text{on PP'} \tag{12}$$

$$\sigma_\theta = \tau_{r\theta} = 0, \quad \text{on PQ and P'Q'} \tag{13}$$

$$u_y^+ = u_y^-, \quad \tau_{xy} = -\tau_Y, \quad \text{on PR and P'R'} \tag{14}$$

where τ_c is the cohesive stress, μ is the coefficient of friction, τ_Y is the yield stress in shear. The principal stresses at infinity are prescribed to be σ_1 and σ_2. The stresses at the ends of the plastic zones must be bounded. Hence we have

$$K_{II} = 0, \quad \text{at R and R'.} \tag{15}$$

Formulation

For the formulation of the boundary-value problem stated above, Muskhelishvili's complex stress function Φ and Ψ are employed. We introduce stress functions $\Phi^D=\Phi_0+\Phi_R$ and $\Psi^D=\Psi_0+\Psi_R$ for a pair of antisymmetric dislocations, and $\Phi^\infty=\Phi_0^\infty+\Phi_R^\infty$ and $\Psi^\infty=\Psi_0^\infty+\Psi_R^\infty$ for stresses at infinity which satisfy

$$\tau_0 + \tau_R = \mu\sigma_0, \quad \sigma_R = 0, \tag{16}$$

$$\tau_{xy}^\infty + \tau_R^\infty = -\tau_c + \mu\sigma_y^\infty, \quad \sigma_R^\infty = 0, \tag{17}$$

where σ_0 and τ_0 are the normal and shear stresses corresponding to Φ_0 and Ψ_0; σ_R and τ_R associated with the

supplementary stress function Φ_R and Ψ_R, σ_0^∞ and τ_0^∞ due to Φ_0^∞ and Ψ_0^∞, and σ_R^∞ and τ_R^∞ due to Φ_R^∞ and Ψ_R^∞.

The stress potentials Φ_R and Ψ_R, and Φ_R^∞ and Ψ_R^∞ are obtained by the method of Muskhelishvili; see Horii and Nemat-Nasser[7] for details. From (16) and (17) it is seen that the stress function $\Phi=\Phi^D+\Phi^\infty$ and $\Psi=\Psi^D+\Psi^\infty$ satisfy (12)-2.

Suitably distributed dislocation of densities α_t and α_p are introduced to represent the tension cracks and the plastic zones. The remaining conditions (13) and (14)-2 lead to a system of integral equations for the dislocation density α_t and α_p. Solving this system of equations with (15) we obtain the values of $K_I/\tau_Y\sqrt{\pi c}$, σ_1/τ_Y for assumed values of θ, ℓ_t, ℓ_p and σ_2/σ_1, and given values of ν, μ and τ_c/τ_Y, using the relation between the dislocation density and the stress intensity factors. In what follows numerical results are shown for $\nu=45^o$, $\mu=0.4$, and $\tau_c=0$.

Numerical Results

For a given σ_2/σ_1, $K_I/\tau_Y\sqrt{\pi c}$ and σ_1/τ_Y are calculated as functions of ℓ_p/c, ℓ_t/c, and θ. The orientation θ is chosen such that $K_I/|\sigma_1|\sqrt{\pi c}$ is maximized. Numerical results show that tension cracks emanate from the flaw tips at an angle of about 70^o with respect to the flaw orientation, and then curve and grow towards the direction of maximum compression, which agree with experimental observations. For a fixed σ_2/σ_1 and given values of ℓ_t/c and ℓ_p/c, we obtain $K_I/\tau_Y\sqrt{\pi c}$ and σ_1/τ_Y corresponding to the critical θ. Typical results are shown in Fig. 7, 8.

From numerical results such as shown in Fig. 7a, 8a we obtain a solution curve in the $(\ell_t/c, \ell_p/c)$-plane, by making use of the following fracture criteria:

$$\begin{aligned} &\text{when cracks are growing,} && K_I = K_c \\ &\text{when cracks are stationary,} && 0 < K_I < K_c, \text{ and} \\ &\text{when cracks are closing,} && K_I = 0, \end{aligned} \tag{18}$$

where the fracture toughness K_c is prescribed. The corresponding axial load σ_1/τ_Y is then established from data similar to those shown in Fig. 7b, 8b.

It is seen that different crack and plastic zone growth regimes are obtained for different values of the "ductility"

$$\Delta = K_I/\tau_Y\sqrt{\pi c} \tag{19}$$

which has a profound effect on the general response predicted by the model.

A relation between the crack length and the plastic zone size is established from Fig. 7a, 8a and the fracture criteria (18). A typical example is shown in Fig. 8a for $\sigma_2/\sigma_1 = 0.15$ and $\Delta = 0.02$. The curve starts at the origin. As the axial load is increased, only the plastic zones develop, until the crack nucleation condition, $K_I = K_c$, is attained. This occurs at A when $\varrho_p/c = 0.002$, a negligible value. Upon further increase in axial stress at a constant stress ratio, both the tension cracks and the plastic zones grow monotonically, as the contour corresponding to $K_I/\tau_Y\sqrt{\pi c} = \Delta = 0.02$, form A to B. At B the tension cracks attain their maximum size, after which the plastic zones continue to grow, relaxing the stress field at the crack tips and possibly causing partial crack closure. This occurs at point C, where the stress intensity factor vanishes. From C to D the size of the open portions of the tension cracks is reduced, so that the $K_I = 0$ is maintained. We refer to this type of crack and plastic zone growth regime as the "brittle mode", which is characterized by the initial part of the curve where tension crack growth dominates the plastic flow.

Brittle mode. Similar results are obtained for other values of Δ and σ_2/σ_1. With the curve in the $(\varrho_t/c, \varrho_p/c)$-plane so established, the axial load can be calculated from results similar to those shown in Fig. 7b, 8b. Fig. 9 illustrates the crack and plastic zone growth regimes, and yield the relations between the axial load and the lengths of the crack and the plastic zone for $\Delta = 0.08$. It is seen that tension cracks cease to grow when the plastic zones attain a size comparable with the crack length. The growth of the plastic zones accelerates after the tension cracks attain their maximum length. The maximum length of the tension cracks may be regarded as representing a measure of the underlying brittleness.

Ductile mode. To examine the crack growth regime at greater values of σ_2/σ_1, solution curves for small crack lengths are plotted in Fig. 10. We observe a different

pattern of crack and plastic zone growth when σ_2/σ_1 is increased from 0.25 to 0.275. Here the size of the plastic zones are dominating the crack length from the beginning. A process of this kind characterizes the "ductile mode".

Transitional mode: unstable crack extension. In the brittle mode, the growth of cracks and plastic zones is stable. On the other hand, if the ductility is intermediate ($0.12<\Delta<0.26$) and the stress ratio is small, we have a "transitional mode", which is characterized by large plastic zones developing before crack initiation, and by unstable crack growth, accompanied by the shortening of plastic zones after crack initiation.

In the transitional mode the plastic zones first emerge and grow with increasing axial load until the condition for crack initiation is satisfied. At this stage, tension cracks suddenly grow in an unstable manner, attaining a finite length, while the calculated size of the plastic zones decreases. Typical crack and plastic zone growth regimes are shown in Fig. 11 for $\Delta = 0.16$. The solid and broken lines are equilibrium curves for indicated stress ratios; the solid lines are for stable growth. The dot-dashed lines indicate unstable crack growth accompanied by the shortening of plastic zone length.

Brittle-ductile transition. From the results discussed above in this section, one may seek to quantify the brittle-ductile transition in terms of the variation of the material ductility Δ and the pressure σ_2/σ_1. The maximum length of the tension cracks represents a measure of the brittleness of the process. This maximum length is plotted as a function of σ_2/σ_1 for indicated Δ in Fig. 12. Solid lines correspond to the response in the brittle mode, and broken lines to the response in the transitional mode. The shaded area represents response in the ductile mode. All curves fall quickly with an increasing stress ratio, indicating the effect of pressure in suppressing brittleness. Three different response modes are obtained depending on Δ and σ_2/σ_1. From results of Fig. 12 we may represent these schematically in a brittle-ductile diagram; see Fig. 13.

Comparison with experimental results – A series of model experiments on Columbia resin CR39 plates containing a single flaw is performed for c = 9mm and $\sigma_2/\sigma_1 = 0.025$, 0.05 and 0.1, and for c = 18mm and $\sigma_2/\sigma_1 = 0.1$ and 0.15. The observed maximum crack lengths are plotted in Fig. 12. It is seen that the data for c = 9mm and 18mm fall on the

curves for $\Delta = 0.15$ and 0.1, respectively. From these results it follows that K_I/τ_Y for this material is about $0.8\sqrt{mm}$.

Experiments on actual rock samples have shown the response in triaxial compression to change from brittle to ductile as the confining pressure is increased. Mogi[8] has summarized experimental data for different rocks; see Fig. 14. The ultimate strength of the specimen with brittle failure is marked with solid symbols. The stresses corresponding to the knee of the stress-strain curve are plotted with open and semi-solid symbols for the ductile response and the transitional response, respectively. It is seen that an increase in the stress ratio from 0.2 to 0.3 results in a change from brittle failure to ductile deformation. Our analytical results are in accord with this feature.

Acknowledgement. This work is supported by the U.S. Air Force of Scientific Research grant no. AFOSR-84-0004 to Northwestern University and the Grant-in Aid for Scientific Research from the Japanese Ministry of Education, Science and Culture. One of the authors (H.H.) wishes to thank Mr. Francois Doremieux, a graduate student, who has helped with calculations in the first part of this work.

REFERENCE

[1] Ramulu, M. and Kobayashi, A.S., Int. J. Fracture, 27 (1985) 187-201.

[2] Dempsey, J.P. and Burgers, P., Int. J. Fracture, 27 (1985) 203-213.

[3] Ravi-Chandar, K. and Knauss, W.G., Int. J. Fracture, 26 (1984) 141-154.

[4] Horii, H., Hasegawa, A. and Nishino, F., Proc. ECF6, (1986).

[5] Horii, H., Hasegawa, A. and Nishino, F., Structural Eng./Earthquake Eng., Japan Society of Civil Eng., Vol. 3, No. 2, 1986.

[6] Lo, K.K., J. Appl. Mech., 45 (1978) 797-802.

[7] Horii, H. and Nemat-Nasser, S., Phil. Trans. R. Soc. Lond., (1986).

[8] Mogi, K., Bull. Earthq. Res. Inst., 44 (1966) 215-232.

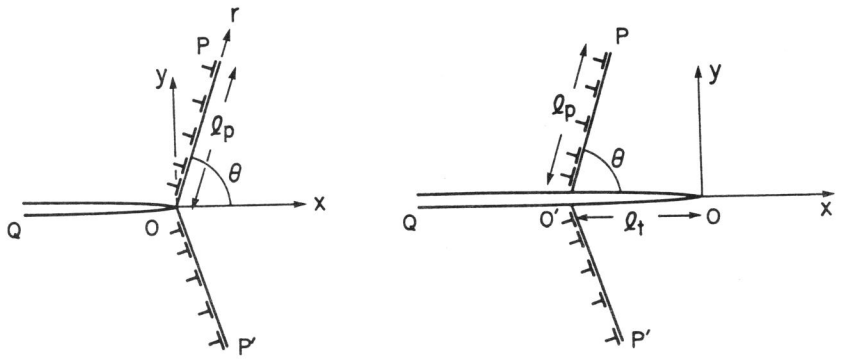

Fig. 1 (a) Planes OP,OP' of the plastic flow at the tip of a semi-infinite crack OQ, and (b) the extended crack OQ with the residual strain along the plastic zones O'P,O'P'.

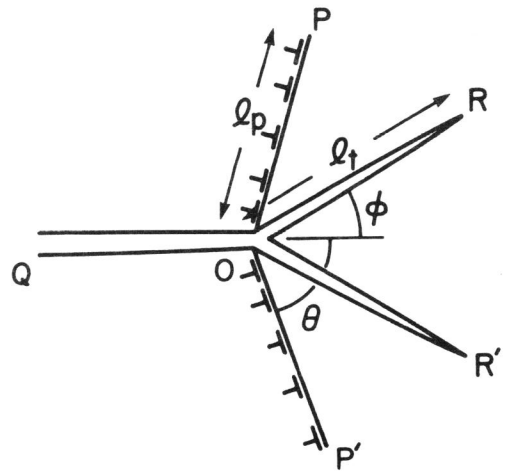

Fig. 2 The branched crack OR,OR' with the residual strain along the plastic zones OP,OP' at the tip of a semi-infinite crack OQ.

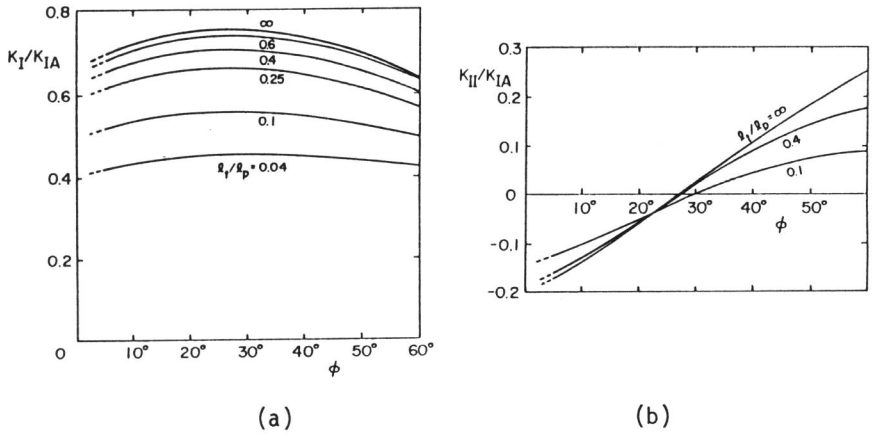

(a) (b)

Fig. 3 (a) The mode I and (b) mode II stress intensity factors at the tip of the branched crack as functions of the branch angle.

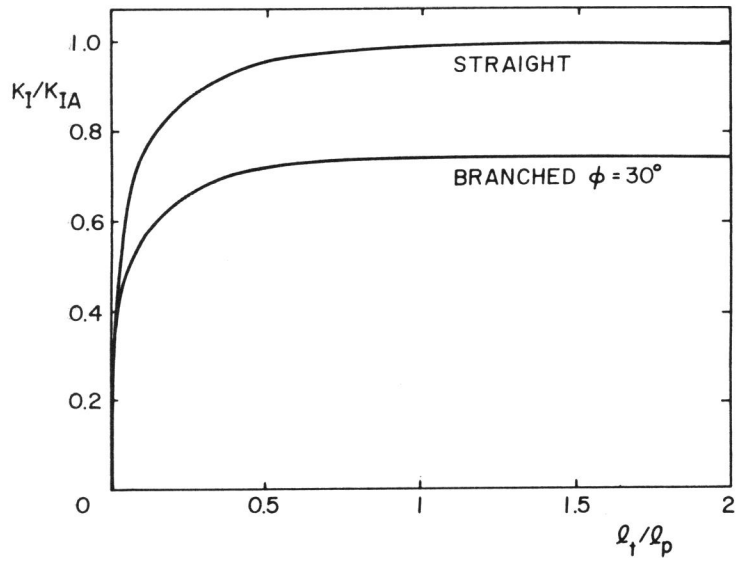

Fig. 4 The mode I stress intensity factor at the branched crack tip and that for the straight crack extension as a function of ℓ_t/ℓ_p.

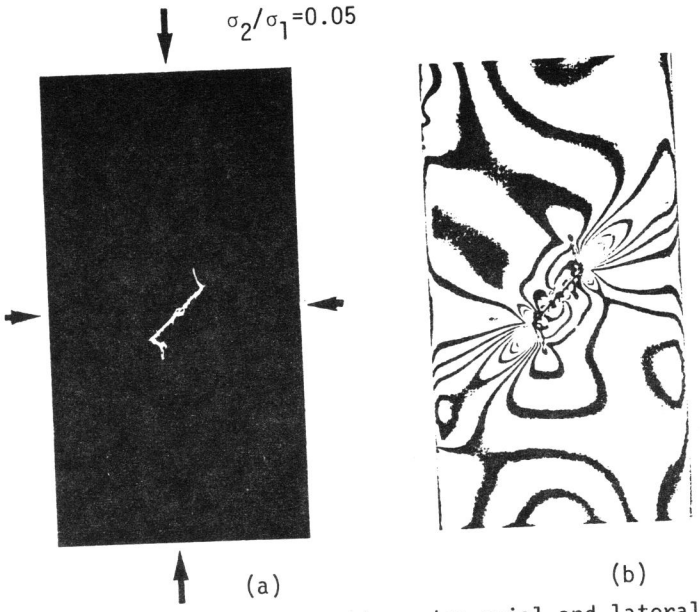

Fig. 5 (a) Arrested tension cracks under axial and lateral compression.
(b) Photoelastic picture of the unloaded specimen.

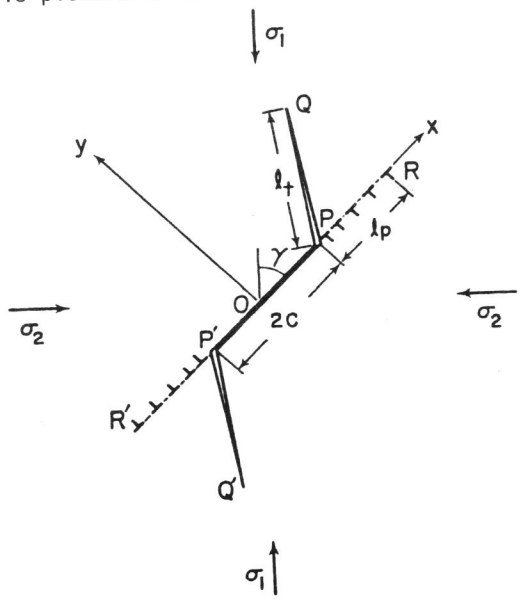

Fig. 6 Model of brittle-ductile transition with a pre-existing flaw PP', tension cracks PQ and P'Q', and plastic zones PR and P'R'.

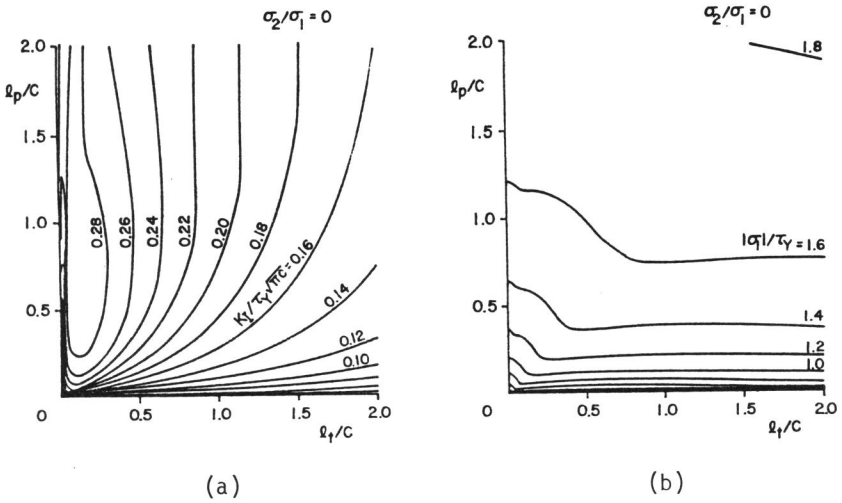

Fig. 7 Contours of constant (a) $K_I/\tau_Y\sqrt{\pi c}$ and (b)σ_1/τ_Y in the ℓ_t,ℓ_p-plane.

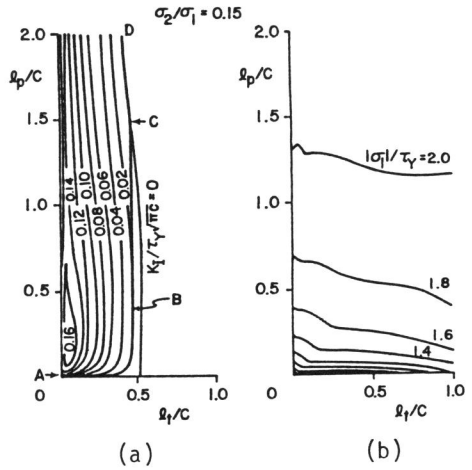

Fig. 8 Contours of constant (a) $K_I/\tau_Y\sqrt{\pi c}$ and (b)σ_1/τ_Y in the ℓ_t,ℓ_p-plane.

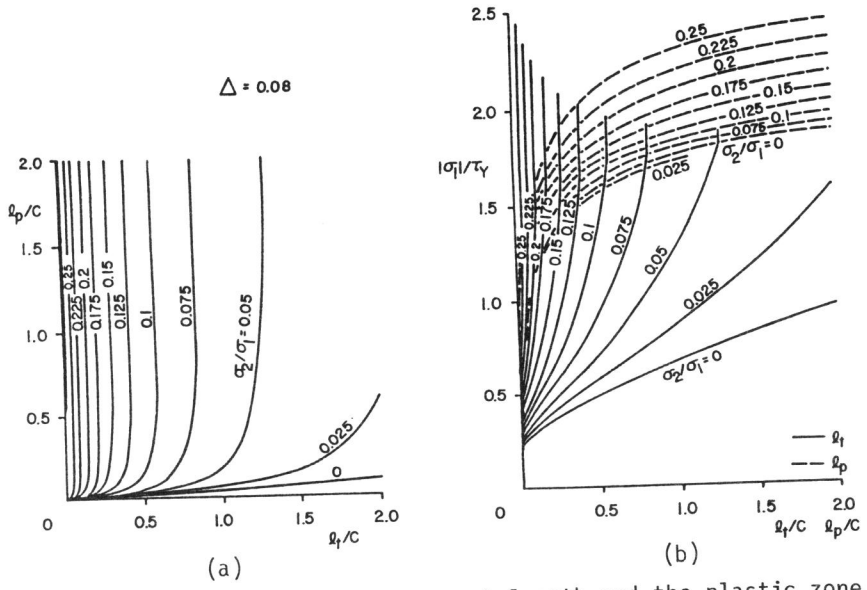

Fig. 9 (a) Relation between the crack length and the plastic zone size under the proportional loading. (b) The corresponding relation between the axial load and the lengths of the crack and the plastic zone.

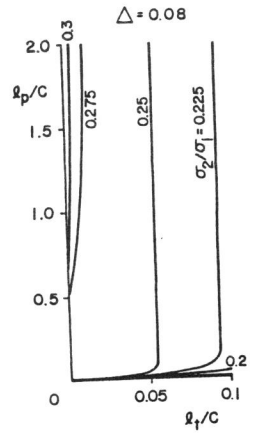

Fig. 10 Relation between the crack length and the plastic zone size; transition from brittle mode to ductile mode.

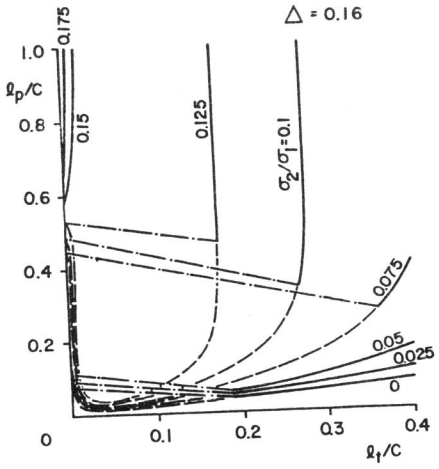

Fig. 11 Relation between the crack length and the plastic zone size; transitional mode - unstable crack extension.

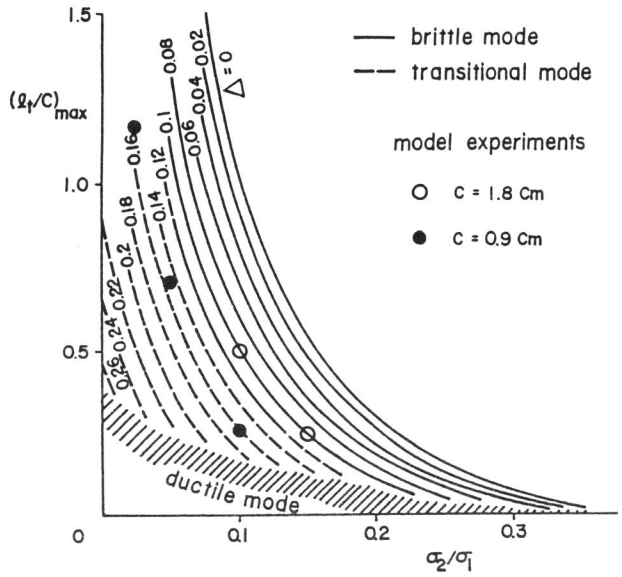

Fig. 12 Maximum crack length as a function of the stress ratio for indicated ductilities; circles are the result of model experiments.

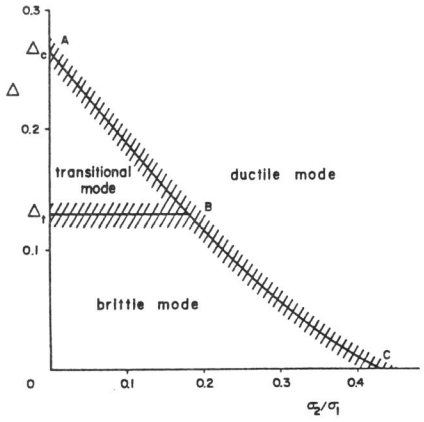

Fig. 13 Brittle-ductile diagram.

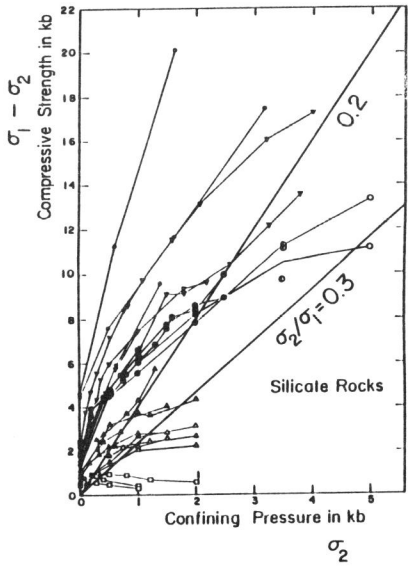

Fig. 14 Variation of compressive strength with confining pressure (From Mogi[8]).